scientific reports

Check for updates

OPEN

# Catalytic synthesis of new pyrazolo [3,4-*b*] pyridine via a coopera tive vinylogous anomeric-based oxidation

Hassan Sepehrmansourie[1], Mahmoud Zarei[1]✉, Mohammad Ali Zolfigol[1]✉, Saeed Babaee[1], Saeid Azizian[2] & Sadegh Rostamnia[3]

**In this study, a novel nano-magnetic metal–organic frameworks based on $Fe_3O_4$ namely $Fe_3O_4$@ MIL-101(Cr)-N($CH_2PO_3$)$_2$ was synthesized and fully characterized. The prepared sample was used as catalyst in the synthesis of pyrazolo [3,4-*b*] pyridines as convenient medicine by condensation reaction of aldehydes, 5-(1*H*-Indol-3-yl)- 2*H*-pyrazol-3-ylamine and 3-(cyanoacetyl)indole via a CVABO. The products were obtained with high yields at 100 °C and under solvent-free conditions.**

Nowadays, rational design, synthesis and catalytic systems is an important topic in the research and development (R&D) of the chemical industries[1–6]. Nanoarchitectonics are methods for introducing nanoporous materials such as magnetic-based ones with high surface area[7–9]. Metal–organic frameworks (MOFs) as nanoporous materials have been widely applied in magnetic resonance imaging (MRI)[10,11], catalysis[12–24], biotechnology[25], gas separation[26], adsorption[27], purification[28], drug delivery[29], etc. The heterogeneous materials based on metallic nanoparticles can play a crucial role in organic synthesis, and have unique properties such as high surface area, easy separation and support for liquid tags materials[30–33]. Therefore, metal–organic frameworks (MOFs) are one of the basic materials for the catalytic preparation of many important molecules in organic synthesis[34–39]. Recently, the synthesis of $Fe_3O_4$ nanomagnetic-based metal–organic frameworks (MOFs) gained attention[40,41]. Because these nanomagnetic-based MOFs catalytic systems have no limitations such as tedious separation and purification[42–45].

In recent years, many quests have been proceeded to investigate the biological and pharmaceutical properties of the nucleus with indole moieties. We have reviewed the reported methodologies for the synthesis of bis- and trisindolylmethanes[46]. Shiri has comprehensively reviewed the application of indoles in the multicomponent processes[47]. In this regard, fused *N*-heterocycles such as pyridines containing of indole moieties may be suitable candidates for biological and pharmacological chemistry investigations[48,49]. Because, *N*-heterocycles have been used as a drug candidate for antimicrobial, cancer, malaria, anticonvulsant, antifungal, HIV, anti-tumor, antioxidant, antihypertension and urinary incontinence treatment[50,51]. Furthermore, pyridine structure kernels are present in pharmaceutical materials and natural products[52]. Among the *N*-heterocycle compounds, pyrazolo[3,4-*b*] pyridine scaffold is the valuable scaffold of material drugs and KDR kinase inhibition[53,54]. Recent research in material chemistry confirmed that pyrazolo[3,4-*b*] pyridine compounds are key intermediates in industry, semiconductors and organic light-emitting diodes[55].

Anomeric effect (AE) as a fundamental example of stereoelectronic interaction has a great educational and research importance. It was discovered in 1955 by J. T. Edward in his studies of carbohydrate chemistry. Historically, this phenomenon was introduced to explain unusual conformational preferences in carbohydrates where the presence of endocyclic oxygen in a glycoside leads to an "abnormal" axial conformational preference for certain substituents at the anomeric carbon[56,57]. In an extension of the classic anomeric effect, a vinyl heteroatom is able to donate electron density from its lone pair through an adjacent π orbital and into the accepting σ* orbital on the other end of the double bond (Fig. 1a).

The anomeric effect can be used as a powerful tool for the justification and interpretation of unusual molecular activities. For example, the forced alignment of three nitrogen non-bonding orbitals with the central antibonding

[1]Department of Organic Chemistry, Faculty of Chemistry, Bu-Ali Sina University, Hamedan 6517838683, Iran. [2]Department of Physical Chemistry, Faculty of Chemistry, Bu-Ali Sina University, Hamedan 6517838683, Iran. [3]Organic and Nano Group (ONG), Department of Chemistry, Iran University of Science and Technology (IUST), PO Box 16846-13114, Tehran, Iran. ✉email: mahmoud8103@yahoo.com; zolfi@basu.ac.ir; mzolfigol@yahoo.com

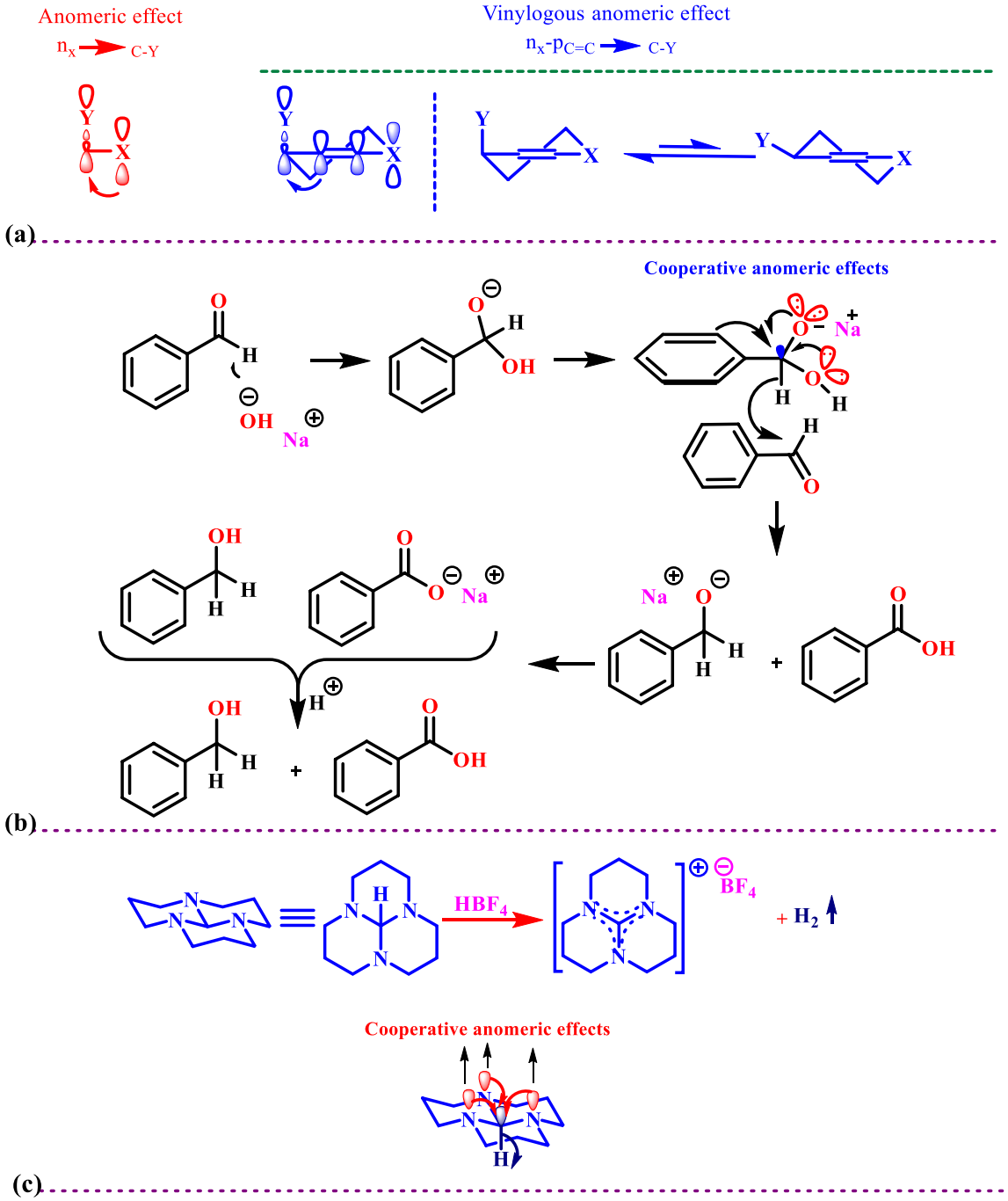


**Figure 1.** (**a**) Anomeric effect versus the vinylogous anomeric effect. (**b**) A (CABO) leads to hydride transfer in the mechanism of the Cannizzaro reaction. (**c**) Hydrogen releasing supported via a cooperative anomeric effect in the orthoformamide (perhydro-3a,6a,9a-triazaphenalene).

$\sigma^*_{C-H}$ orbital within the ortho formamide and cooperative anomeric effect weakens the bond and leads to an "unusual" hydride transfer under acidic conditions (Fig. 1b)[58–61].

Recently the term ABO has been introduced[62,63] and reviewed[64,65]. A famous example of ABO is the Cannizzaro reaction via the addition of hydroxide ($OH^-$) to the carbonyl group of aldehydes which do not have $\alpha$-hydrogen (Fig. 1c), both of the lone pair's electrons of oxygen atoms within the tetrahedral carbon sharing their electrons into the anti-bonding orbital of C–H bond ($n_N \rightarrow \sigma^*_{C-H}$) and weakened it. The resulting labile hydride acts as a powerful nucleophile that attacks to the second molecule of aldehyde. Finally, this reaction produced equal amounts of the corresponding alcohol and acid.

According to the strategy of expanding compounds with biological activities, we have introduced a novel $Fe_3O_4$@MIL-101(Cr)-$N(CH_2PO_3)_2$ as a catalyst. This magnetic metal–organic framework was used in the

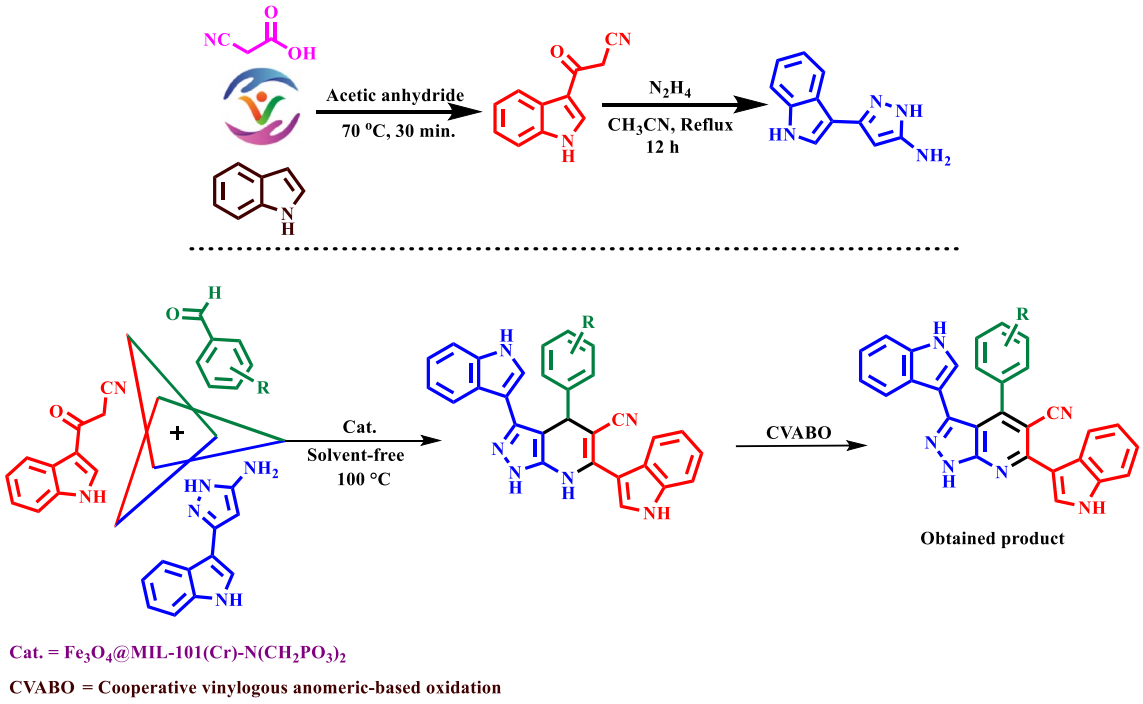


**Figure 2.** Preparation of novel mono and bis and tris pyrazolo[3,4-*b*] pyridine using $Fe_3O_4$@MIL-101(Cr)-N($CH_2PO_3$)$_2$ as catalyst.

synthesis of novel mono, bis and tris pyrazolo [3,4-*b*] pyridines with both indole and pyrazole moieties at 100 °C in solvent-free conditions (Fig. 2).

## Experimental

**Synthesis of $Fe_3O_4$@MIL-101(Cr)-N($CH_2PO_3$)$_2$ as catalyst.** According to the previously reported methods, MIL-101(Cr)-$NH_2$ and MIL-101(Cr)-N($CH_2PO_3H_2$)$_2$ were synthesized[66–68]. Then a mixture of MIL-101(Cr)-N($CH_2PO_3H_2$)$_2$ (1.3 g) and $Fe_3O_4$ (1 g) were dispersed in toluene at 80 °C for 12 h. After cooling the reaction mixture, the nano-magnetic metal–organic framework $Fe_3O_4$@MIL-101(Cr)-N($CH_2PO_3$)$_2$ was separated by an external magnet and washed with ethanol for several times (Fig. 3).

**General method for the preparation of pyrazolo[3,4-*b*] pyridines.** Firstly, the raw materials 3-(cyanoacetyl) indole and 5-(1*H*-Indol-3-yl)-2*H*-pyrazol-3-ylamine were synthesized according to the previously literature reported procedures (Fig. 2)[69,70]. Then, a mixture of aldehyde derivatives (1 mmol), 5-(1*H*-Indol-3-yl)-2*H*-pyrazol-3-ylamine (0.198 g, 1 mmol), 3-(cyanoacetyl) indole (0.184 g, 1 mmol) and nano-magnetic metal–organic frameworks $Fe_3O_4$@MIL-101(Cr)-N($CH_2PO_3$)$_2$ as catalyst (20 mg) were mixed and stirred at 100 °C. Progress of the reaction was followed by applying the TLC technique. After completing the reaction, the reaction system was cooled to 25 °C. Then, hot ethanol was added to the reaction mixture, and the catalyst was removed from the reaction mixture with an external magnet. The ethanol was evaporated, and finally, the pyrazolopyridine product was purified by plate chromatography (EtOAc/*n*-hexane:1/1). $^1$H NMR (400 MHz, DMSO-$d_6$), $^{13}$C NMR (100 MHz, DMSO-$d_6$), FT-IR (KBr, cm$^{-1}$) and melting point analysis were used for all synthesized molecules.

## Result and discussion

Nowadays, synthesized molecules bearing pyridine-based scaffolds with indole moieties are attracted the attention of pharmaceutical chemistry researchers due to their building block's ability in pharmaceuticals and modern drug design approaches. So, there still is a great demand for the introducing of more practical and facile procedures and catalytic systems for multicomponent reactions in the organic synthesis field. On the other hand, the joining of indole, pyridine, and pyrazole moieties within a single molecule is our main research proposal in this investigation. We think that combining of above-mentioned units in a single structure can open up a new and promising insight in the course of rational design, synthesis and applications of drug candidate compounds. According to our recent findings[71–78], we believed that the stereoelectronic effect has a major role in the last step of the proposed mechanism. To the best of our knowledge and literature surveys, there is no report on the synthesis of described pyridines. Therefore, herein we wish to report the first catalytic and multicomponent method for the preparation of new pyridines with both pyrazole and indole aromatic moieties via CVABO.

In order to extend the field of magnetic metal–organic frameworks catalysts, our research group has presented and synthesized a novel MIL-101(Cr)-N($CH_2PO_3H_2$)$_2$ connected to $Fe_3O_4$ tags (Fig. 2). The structure of $Fe_3O_4$@MIL-101(Cr)-N($CH_2PO_3$)$_2$ as a magnetic metal–organic frameworks catalyst was characterized by FT-IR, XRD,

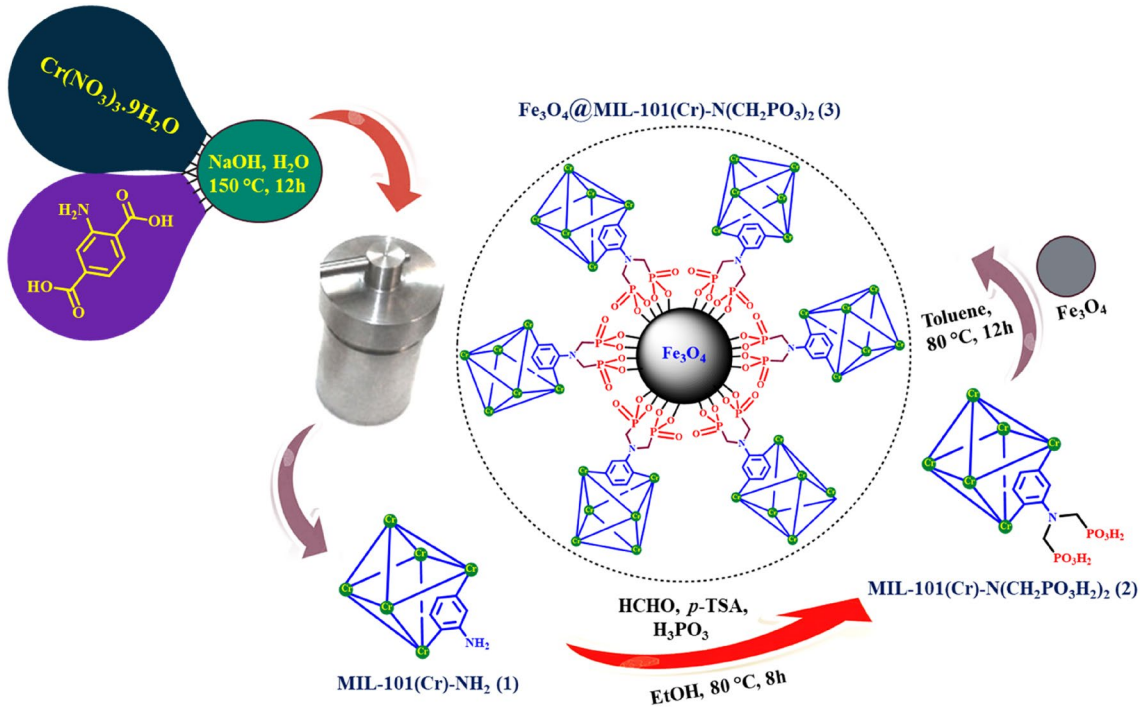


**Figure 3.** Preparation of nano-magnetic metal–organic frameworks catalyst.

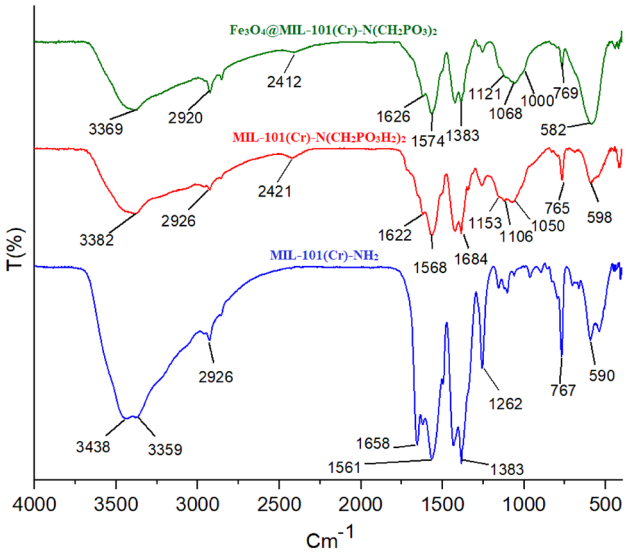


**Figure 4.** FT-IR spectra of catalyst and starting materials.

SEM, EDX, SEM-elemental mapping, TG, DTG and $N_2$ adsorption–desorption isotherm (BET analysis). Then, the magnetic metal–organic frameworks catalyst was applied for the preparation of novel pyrazolo[3,4-*b*] pyridine derivatives as biological candidates.

The FT-IR spectra of $Fe_3O_4$@MIL-101(Cr)-N$(CH_2PO_3)_2$ as the catalyst, MIL-101(Cr)-N$(CH_2PO_3H_2)_2$ and MIL-101(Cr)-$NH_2$ were shown in Fig. 4. The broadband at 2600–3500 $cm^{-1}$ is related to OH of $PO_3H_2$ functional groups in MIL-101(Cr)-N$(CH_2PO_3H_2)_2$. The peaks P–O and P=O bond stretching are shown in 1000 $cm^{-1}$, 1068 $cm^{-1}$ and 1121 $cm^{-1}$ respectively. Also, the absorption peaks at 2920 and 1626 $cm^{-1}$ are related to aromatic C–H and C=C stretching bands. Furthermore, the peak at 582 $cm^{-1}$ is related to the stretching vibrational modes of Fe–O groups in $Fe_3O_4$. The FT-IR difference between starting materials and $Fe_3O_4$@MIL-101(Cr)-N$(CH_2PO_3)_2$ as catalyst verified the scaffold of the catalyst.

The particle size and phase of $Fe_3O_4$@MIL-101(Cr)-N$(CH_2PO_3)_2$ as catalyst and MIL-101(Cr)-N$(CH_2PO_3H_2)_2$ were investigated by XRD at the range of 5–80°, Fig. 5. The XRD patterns demonstrated diffraction lines of high crystalline nature at $2\theta = 18.0°$, 30.3°, 35.5°, 43.6°, 54.0°, 57.3°, 62.7° and 74.6° correspond to the $Fe_3O_4$ diffraction lines (111), (220), (311), (400), (422), (511), (440) and (533) (Fig. 5)[79]. Also, the Scherer equation

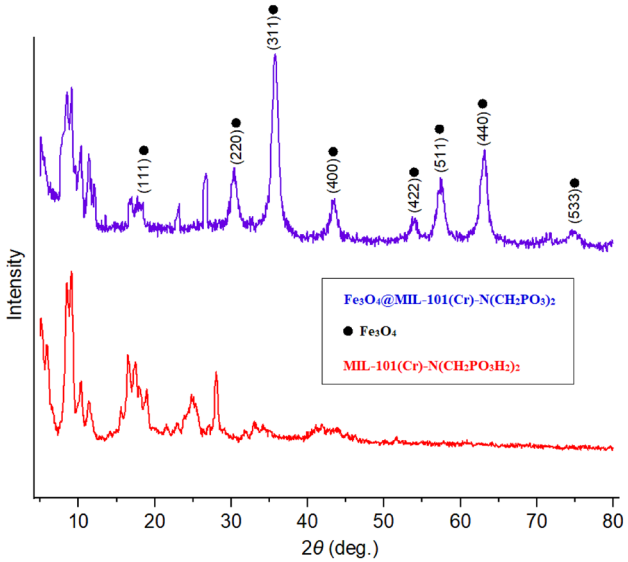


**Figure 5.** Comparison XRD pattern of catalyst and MIL-101(Cr)-$N(CH_2PO_3H_2)_2$ as starting material.

| Entry | 2θ | Peak width (degree) | Size [nm] | Inter planer distance [nm] |
|---|---|---|---|---|
| 1 | 8.20 | 0.30 | 26.4 | 1.074 |
| 2 | 23.15 | 0.55 | 14.6 | 0.383 |
| 3 | 26.80 | 0.55 | 14.7 | 0.331 |
| 4 | 30.55 | 1.6 | 5.1 | 0.291 |
| 5 | 35.70 | 1.15 | 7.2 | 0.251 |
| 6 | 43.40 | 0.67 | 12.6 | 0.208 |
| 7 | 57.55 | 1 | 9.0 | 0.160 |
| 8 | 63.05 | 1 | 9.2 | 0.147 |

**Table 1.** XRD data of catalyst.

and Bragg equation were used for the averaged inter planer distance and sizes of crystal, which are determined 5.1–26.4 nm (Table 1).

For further verification of the scaffold and elemental analysis in the prepared catalyst, the energy dispersive X-ray analysis (EDX) analysis was used (Fig. 6a). The constituents of the catalyst were verified with the existence of Fe, N, Cr, O, C and P atoms. Figure 6b shows that the elementals of $Fe_3O_4$@MIL-101(Cr)-$N(CH_2PO_3)_2$ are distributed uniformly.

In another study, the particle size and morphology of $Fe_3O_4$@MIL-101(Cr)-$N(CH_2PO_3)_2$ as catalyst were studied by scanning electron microscope (SEM) (Fig. 7). As shown in Fig. 7 the particles have spherical shape in the nanoscale size.

The $N_2$ adsorption/desorption isotherms were utilized to analyze the textural features of $Fe_3O_4$@MIL-101(Cr)-$N(CH_2PO_3)_2$ (Fig. 8a). A hysteresis loop is observed, indicating the presence of mesopores in the structure of the sample. The calculated surface area (BET) and the total pore volume are 100.03 $m^2\ g^{-1}$ and 0.518 $cm^3\ g^{-1}$, respectively. The plot of the pore size distribution of $Fe_3O_4$@MIL-101(Cr)-$N(CH_2PO_3)_2$ obtained by the BJH method is presented in (Fig. 8a). This plot reveals that the catalyst possesses both micropores (size < 2 nm) and mesopores (2 < size < 50 nm), however, the radius of most of the pores is less than 10 nm. Figure 8b depicts the magnetic measurements of $Fe_3O_4$@MIL-101(Cr)-$N(CH_2PO_3)_2$ and $Fe_3O_4$. The vibrating sample magnetometer (VSM) of $Fe_3O_4$ and $Fe_3O_4$@MIL-101(Cr)-$N(CH_2PO_3)_2$ were compared, the vibrating sample magnetometer of pure $Fe_3O_4$ reduced from 64.5 up to 53.5 $mug^{-1}$ for the $Fe_3O_4$@MIL-101(Cr)-$N(CH_2PO_3)_2$. Therefore, this reduction is for the coating of $Fe_3O_4$@MIL-101(Cr)-$N(CH_2PO_3)_2$ onto the surface of $Fe_3O_4$.

The thermal and behavioral stability of nano-magnetic metal–organic frameworks $Fe_3O_4$@MIL-101(Cr)-$N(CH_2PO_3)_2$ were studied by thermal gravimetric (TG) and derivative thermal gravimetric (DTG) techniques (Fig. 9). The first step is the weight loss, which took place between 25 and 100 °C, associated with the removal of solvents (organic and water). The main stage of weight loss, disrupts the structure of $Fe_3O_4$@MIL-101(Cr)-$N(CH_2PO_3)_2$, took place at 380 °C, and includes about 35% weight loss. Therefore, this catalyst can be used up to 300 °C.

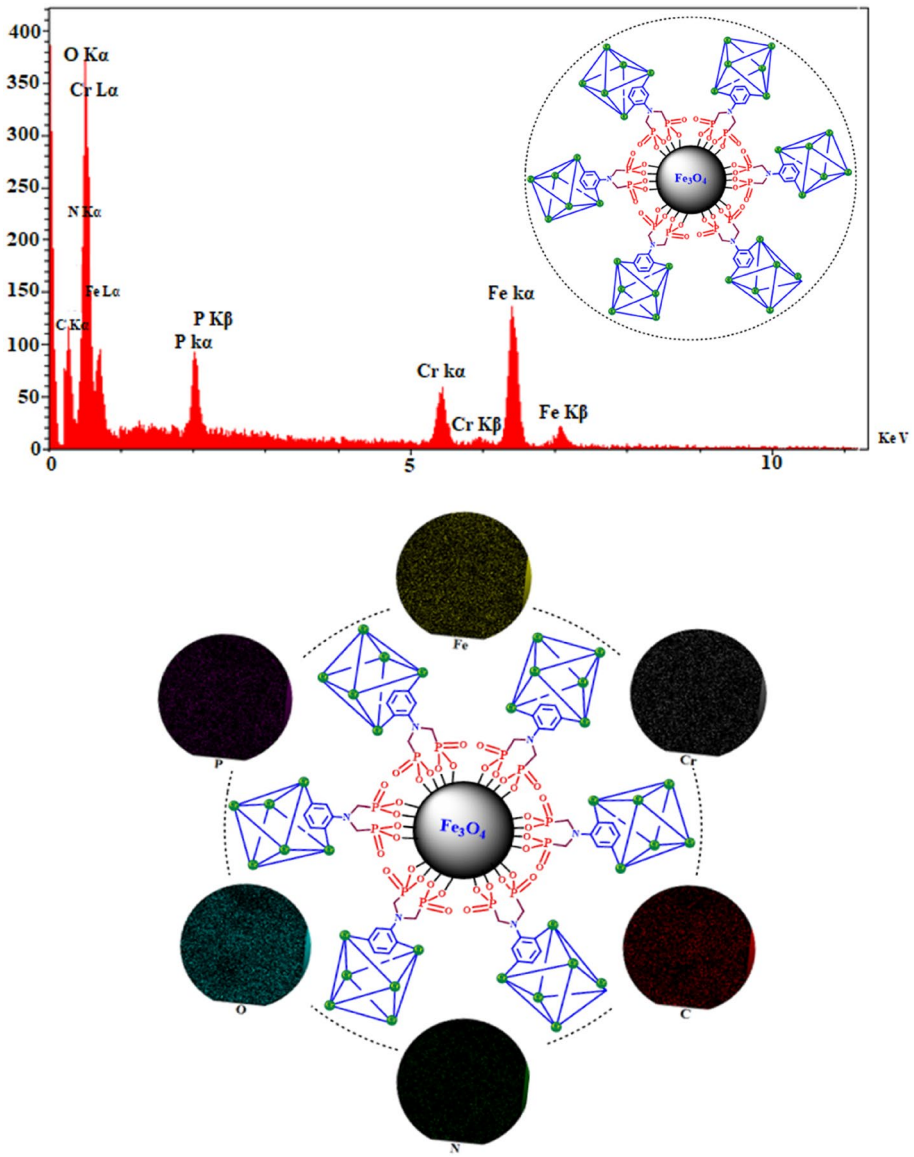


**Figure 6.** $Fe_3O_4$@MIL-101(Cr)-N$(CH_2PO_3)_2$: **(a)** EDX analysis. **(b)** Elemental mapping of C (red), O (blue), N (green), Fe (yellow), P (purple) and Cr (gray) atoms.

After the synthesis and characterization of $Fe_3O_4$@MIL-101(Cr)-N$(CH_2PO_3)_2$, it was used for the synthesis of new pyrazolo [3,4-*b*] pyridine derivatives with indole and pyrazole tags. The mentioned compounds were prepared by reaction of 4-chloro benzaldehyde (0.141 g, 1.0 mmol), 5-(1*H*-Indol-3-yl)-2*H*-pyrazol-3-ylamine (0.198 g, 1 mmol) and 3-(cyanoacetyl) indole (0.184 g, 1 mmol) as a suitable model for the optimization the reaction conditions. The results are assembled in Table 2, the best option for the preparation of compound C2 was achieved in the presence of 20 mg $Fe_3O_4$@MIL-101(Cr)-N$(CH_2PO_3)_2$ in solvent-free conditions (Table 2, entry 2). The target reaction was also examined by using several solvents such as DMF, $CH_3CN$, MeOH, $H_2O$, EtOH, $CH_2Cl_2$, $CHCl_3$, and EtOAc (5 mL) in the presence of 20 mg of catalyst. The reaction results did not improve (Table 2, entries 9–17). These interesting results encouraged us to synthesis a wide range of pyrazolo [3,4-*b*] pyridine compounds in solvent-free conditions.

As above-mentioned, after optimizing the reaction conditions, catalyst (20 mg) is used for the preparation of new biomolecules products using widespread aldehydes such as bearing electron-donating, electron-withdrawing groups, iso-trephetaldehyde and tris-aldehyde, 5-(1*H*-Indol-3-yl)-2*H*-pyrazol-3-ylamine and 3-(cyanoacetyl) indole. The results can be seen in Table 3, the obtained results show that the prepared catalyst is suitable for the synthesis of mono, bis and tris products with high yields (70–90%) and short reaction time (35–60 min).

In the suggested mechanism, the catalyst activates the carbonyl group of aldehyde. Firstly, intermediate (**I**) as a Michael acceptor is produced by the reaction of activated aldehyde and 3-(cyanoacetyl)indole. In the next step, intermediate (**II**) is prepared from reactions of 5-(1*H*-Indol-3-yl)-2*H*-pyrazol-3-ylamine and intermediate (**I**). In the third step, intermediate (**III**) is obtained by cyclization and losing one molecule of $H_2O$. Then, intermediate (**III**) via interaction of lone pair electrons of N atoms from C=C bonds causes the release hydride

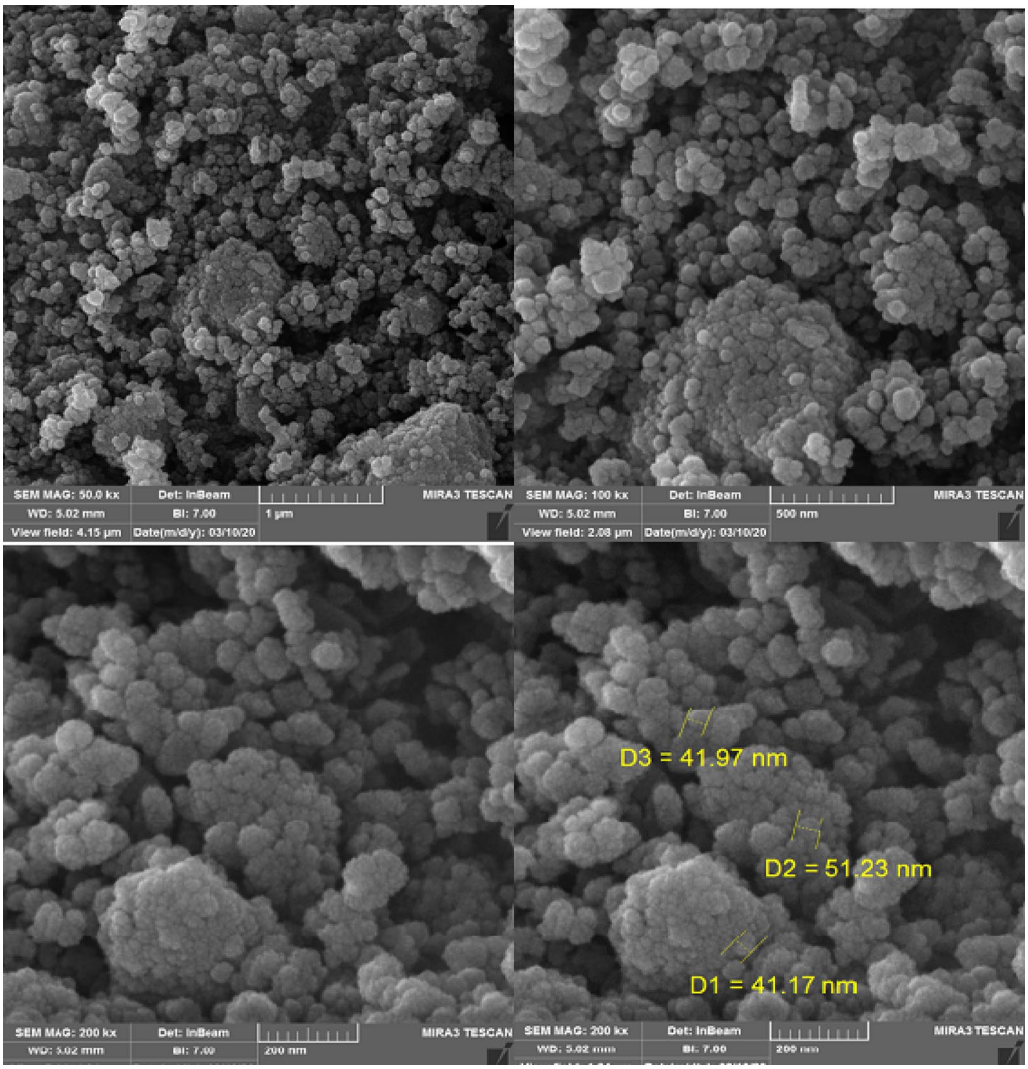


**Figure 7.** Scanning electron microscope (SEM) images of catalyst.

and $H_2$. Finally, the 1,4-dihydropyridines convert to their corresponding pyrazolo [3,4-*b*] pyridine derivatives via a CVABO and release a hydrogen molecule ($-H_2$)[80,81]. The optimization of model reaction under argon and $N_2$ atmospheres are also verified the desired product (Fig. 10). To investigate the activation of aldehyde by catalyst, *p*-chloro benzaldehyde was activated with $Fe_3O_4$@MIL-101(Cr)-$N(CH_2PO_3)_2$ at room temperature. Then the FT-IR spectra of the reaction mixtures were examined. The absorption band of C=O of the *p*-chloro benzaldehyde at 1708 $cm^{-1}$ was changed to 1702, 1698, 1698 $cm^{-1}$ in the presence of MIL-101(Cr)-$N(CH_2PO_3)_2$, MIL-101(Cr)-$NH_2$ and $Fe_3O_4$ (Fig. 11).

To compare the efficiency of the synthesized catalyst in the preparation of pyrazolo [3,4-*b*] pyridine derivatives, the model reaction (compound C2) was tested using various inorganic and organic catalysts under optimal conditions (Table 4). As Table 4 shows, nano-magnetic metal–organic frameworks $Fe_3O_4$@MIL-101(Cr)-$N(CH_2PO_3)_2$ is the best catalyst for the preparation of the desired product. Also, to investigate the heterogeneous nature of the protocols and palladium leaching, ICP/MS results proved that no Fe and Cr leaching was detected in the filtrate (Fe: $2.5 \times 10^{-6}$ and Cr: $1.9 \times 10^{-5}$ mol $g^{-1}$ respectively) upon reaction completion, which indicates the high stability of the prepared catalyst.

Finally, for the reusability of the nano-magnetic metal–organic frameworks $Fe_3O_4$@MIL-101(Cr)-$N(CH_2PO_3)_2$ in the synthesis of pyrazolo[3,4-*b*] pyridine, this catalyst was examined in 3-(cyanoacetyl) indole (0.184 g, 1 mmol), 4-chloro benzaldehyde (0.141 g, 1 mmol) and 5-(1*H*-Indol-3-yl)-2*H*-pyrazol-3-ylamine (0.198 g, 1 mmol) (compound C2) as model reactions. The results show that the prepared catalyst can be reused up to 7 times without noticeable reduction (Fig. 12).

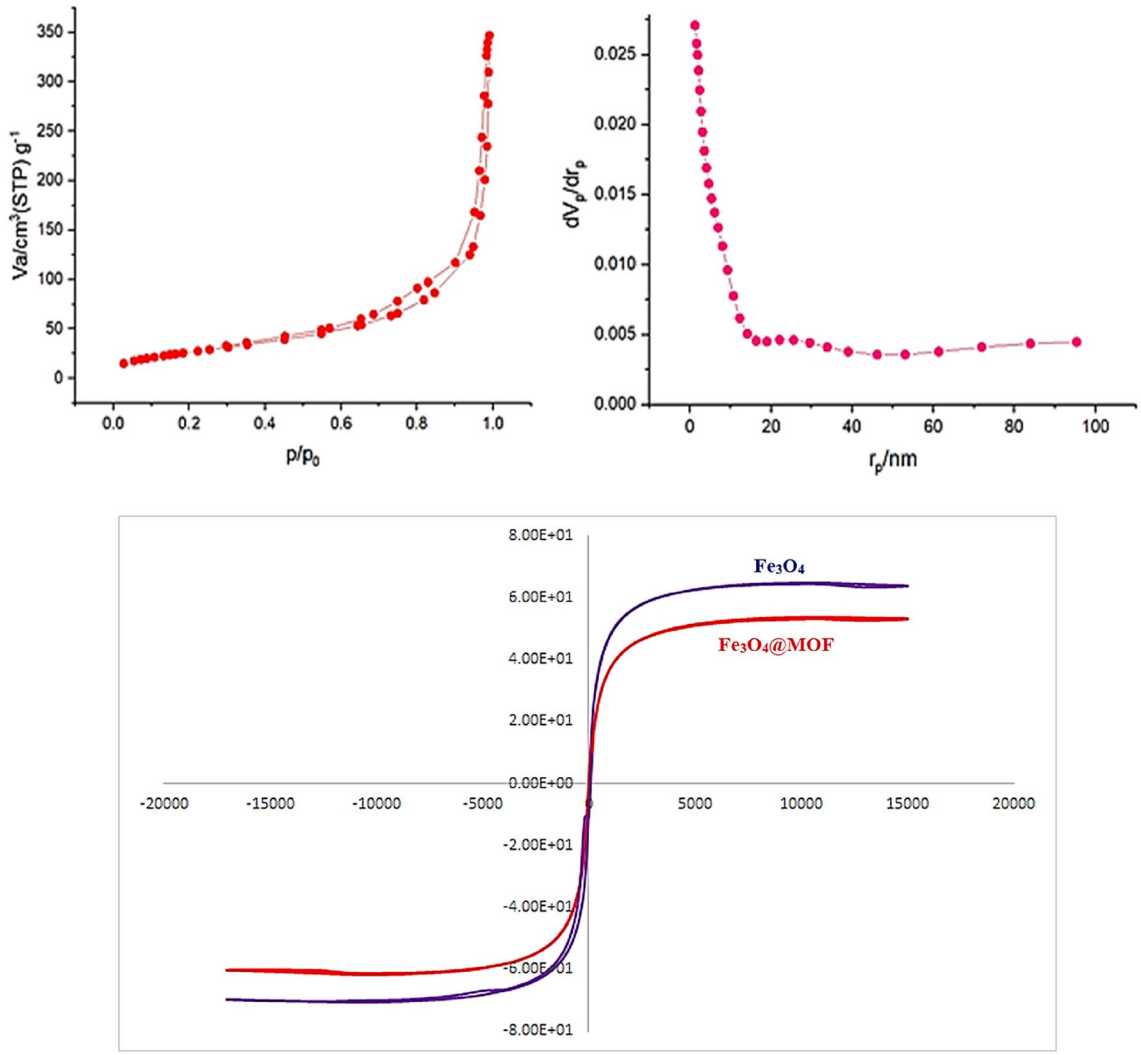


**Figure 8.** $Fe_3O_4$@MIL-101(Cr)-N($CH_2PO_3$)$_2$: (**a**) BET and BJH isotherms, (**b**) VSM.

## Conclusion

In summary, a magnetic metal–organic frameworks $Fe_3O_4$@MIL-101(Cr)-N($CH_2PO_3$)$_2$ as nano-catalyst was designed and synthesized and identified by various techniques such as FT-IR, XRD, SEM, EDX, Mapping, BET and VSM analysis. This catalyst was tested for the preparation of novel pyrazolo[3,4-*b*]pyridines according to (CVABO) concept. The advantages of this work include, synthesis of new pyrazolo[3,4-*b*]pyridines as biological candidates, short reaction time, clean profile of the reaction and catalyst recyclability.

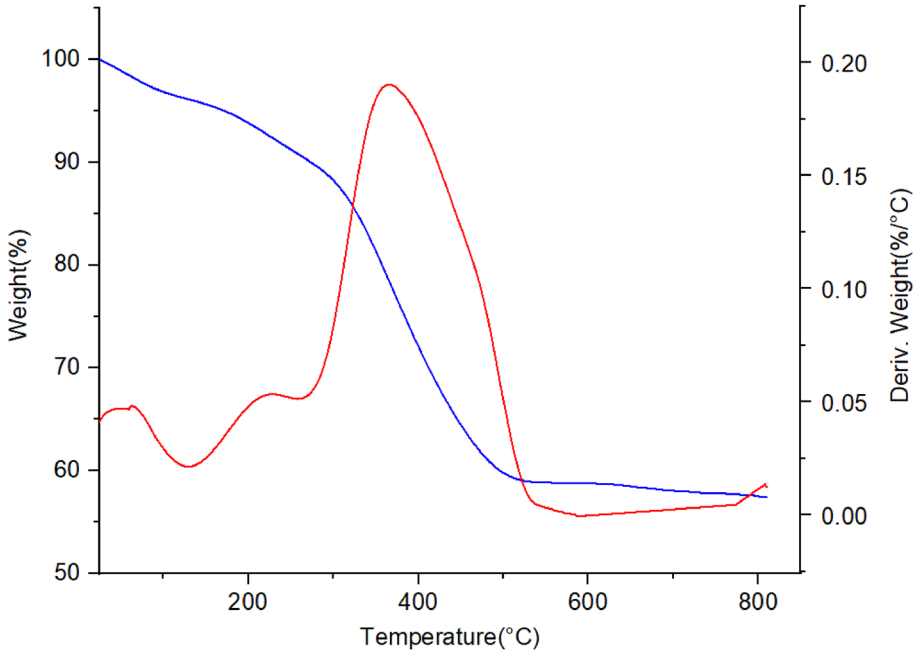


**Figure 9.** Thermal gravimetric (TG) and derivative thermal gravimetric (DTG) analysis of $Fe_3O_4$@MIL-101(Cr)-N($CH_2PO_3$)$_2$.

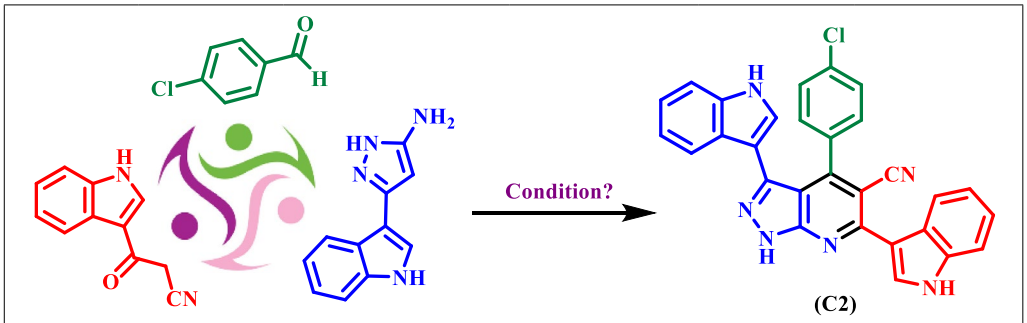


| Entry | Solvent | Catalyst (mg) | Temp. (°C) | Time | Yield (%) |
|---|---|---|---|---|---|
| 1 | – | 20 | 110 | 60 (min) | 80 |
| 2 | – | 20 | 100 | 60 (min) | 87 |
| 3 | – | 20 | 90 | 60 (min) | 82 |
| 4 | – | 20 | 50 | 60 (min) | 10 |
| 5 | – | 20 | 25 | 60 (min) | – |
| 6 | – | 30 | 100 | 60 (min) | 85 |
| 7 | – | 100 | 100 | 60 (min) | 56 |
| 8 | – | 5 | 100 | 60 (min) | 25 |
| 9 | DMF | 20 | Reflux | 7 (h) | 83 |
| 10 | DMF | 20 | 100 | 8 (h) | 82 |
| 11 | $CH_3CN$ | 20 | Reflux | 10 (h) | 38 |
| 12 | MeOH | 20 | Reflux | 8 (h) | 15 |
| 13 | $H_2O$ | 20 | Reflux | 9 (h) | 10 |
| 14 | EtOH | 20 | Reflux | 10 (h) | 45 |
| 15 | $CH_2Cl_2$ | 20 | Reflux | 12 (h) | – |
| 16 | $CHCl_3$ | 20 | Reflux | 12 (h) | – |
| 17 | EtOAc | 20 | Reflux | 10 (h) | – |

**Table 2.** Optimization parameter on the synthesis **C2** compound.

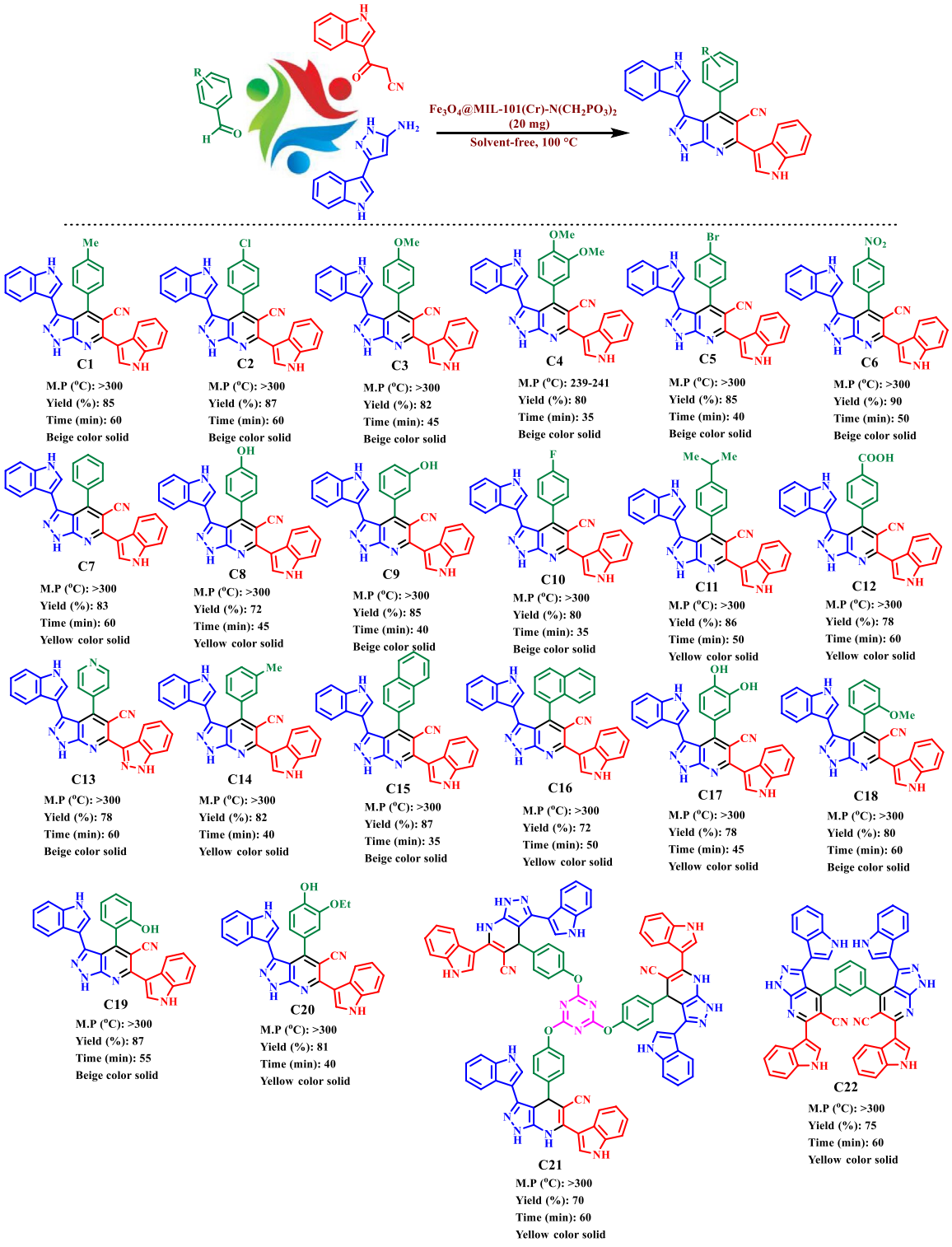


**Table 3.** Synthesis of pyrazolo[3,4-*b*] pyridine derivatives (**C1–C22**) using $Fe_3O_4$@MIL-101(Cr)-N($CH_2PO_3$)$_2$ as a catalyst.

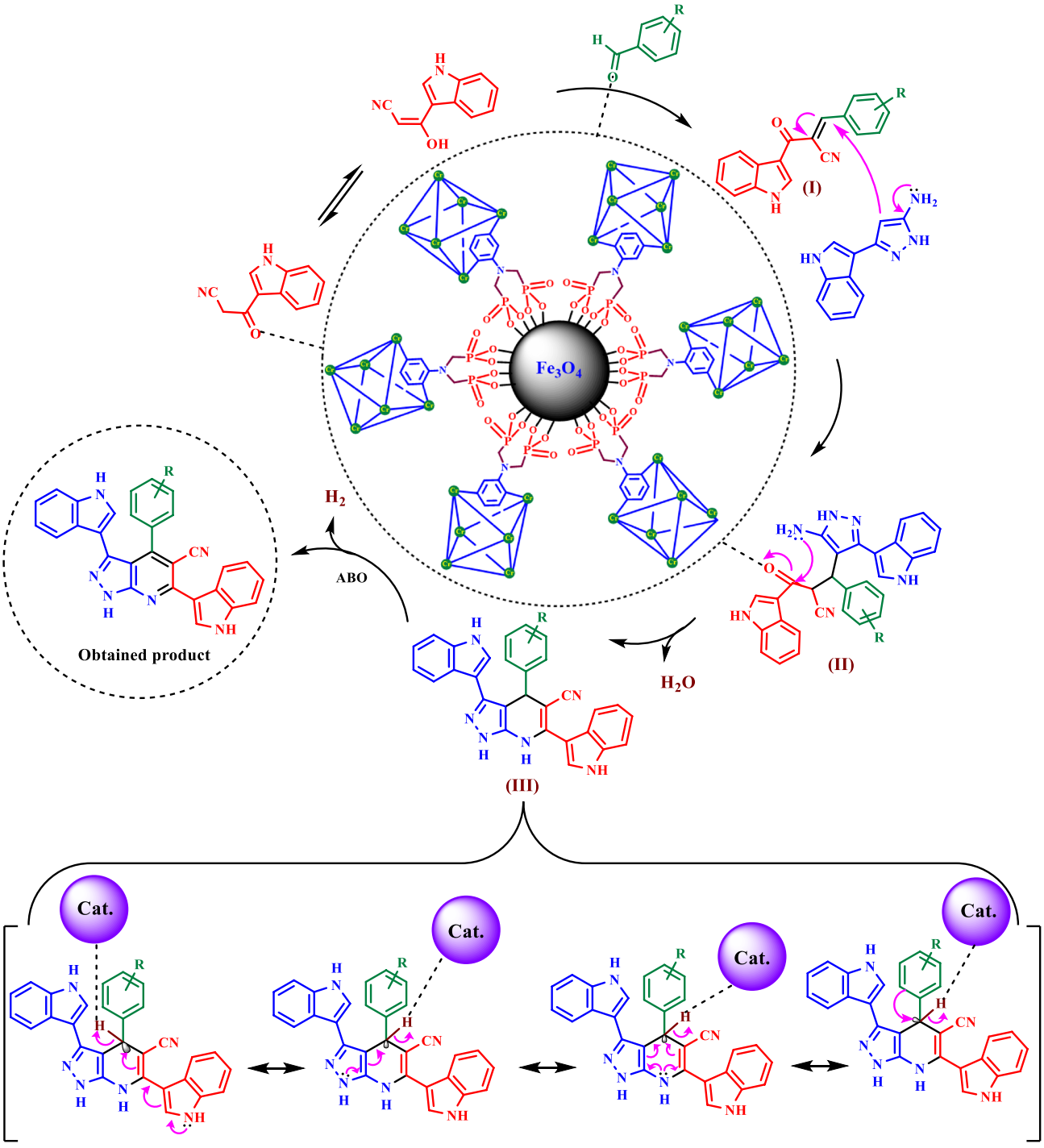


**Figure 10.** Proposed mechanism for the synthesis of pyrazolo[3,4-*b*]pyridine derivatives using $Fe_3O_4$@MIL-101(Cr)-N($CH_2PO_3$)$_2$ as catalyst.

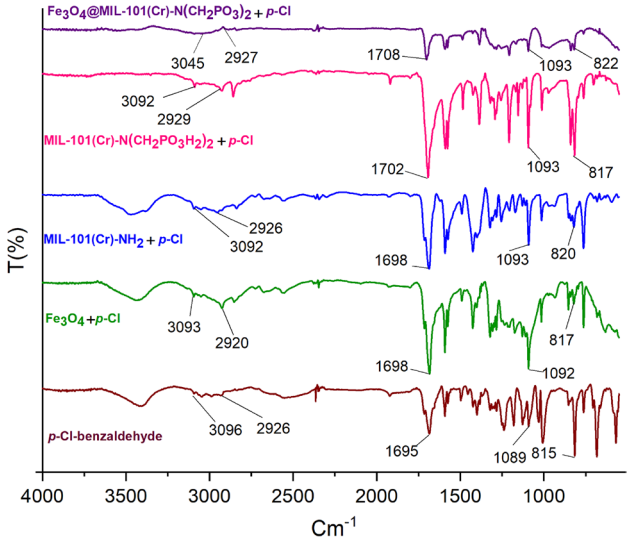


**Figure 11.** FT-IR spectra of *p*-Cl-benzaldehyde in percent of $Fe_3O_4$, MIL-101(Cr)-$NH_2$, MIL-101(Cr)-$N(CH_2PO_3H_2)_2$ and $Fe_3O_4$@MIL-101(Cr)-$N(CH_2PO_3)$.

| Entry | Catalyst | (Mol %) | (Time/min.) | Yield (%) |
|---|---|---|---|---|
| 1 | $FeCl_3$ | 10 | 120 | – |
| 2 | [PVI-$SO_3H$]$FeCl_4$[82] | 10 mg | 120 | 48 |
| 3 | $CF_3SO_3H$ | 10 | 120 | 15 |
| 4 | $H_2SO_4$ | 10 | 120 | 42 |
| 5 | [Py-$SO_3H$]Cl[83] | 10 mg | 120 | 36 |
| 6 | $Fe_3O_4$ | 10 mg | 120 | – |
| 7 | $K_2CO_3$ | 10 | 120 | – |
| 8 | SSA[84,85] | 10 mg | 120 | 20 |
| 9 | $Et_3N$ | 10 | 120 | – |
| 10 | NaOH | 10 | 120 | – |
| 11 | MIL-100(Cr)/NHEtN$(CH_2PO_3H_2)_2$[86] | 10 mg | 120 | 52 |
| 12 | *p*-TSA | 10 | 120 | 25 |
| 13 | GTBSA[87] | 10 | 120 | 40 |
| 14 | MHMHPA[72] | 10 | 120 | 32 |
| 15 | $Fe_3O_4$@MIL-101(Cr)-$N(CH_2PO_3)_2$ (this work) | 20 mg | 60 | 87 |

**Table 4.** Compare of various catalyst for the synthesis of pyrazolo [3,4-*b*] pyridine derivatives in comparison with $Fe_3O_4$@MIL-101(Cr)-$N(CH_2PO_3)_2$.

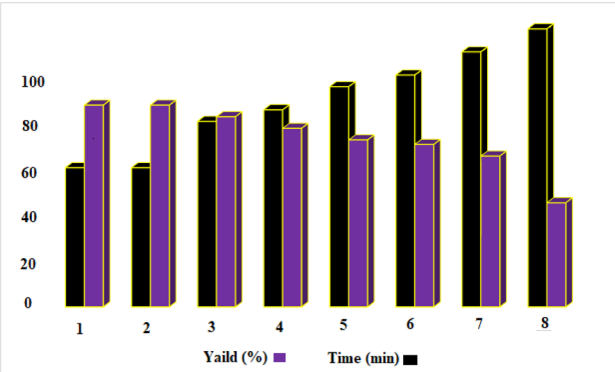


**Figure 12.** Recyclability of catalyst for the synthesis of pyrazolo[3,4-*b*]pyridine derivatives.

## Data availability

The datasets used and/or analyzed during the current study available from the corresponding author on reasonable request.

Received: 27 February 2022; Accepted: 2 August 2022
Published online: 19 August 2022

## References

1. Vojvodic, A. & Norskov, J. K. New design paradigm for heterogeneous catalysts. *Natl. Sci. Rev.* **2**, 140–143 (2015).
2. Hu, X., Zhu, H., Sang, X. & Wang, D. Design and synthesis of zirconium-containing coordination polymer based on unsymmetric indolyl dicarboxylic acid and catalytic application on borrowing hydrogen reaction. *Adv. Synth. Catal.* **360**, 4293–4300 (2018).
3. Rossi, R., Angelici, G., Casotti, G., Manzini, C. & Lessi, M. Catalytic synthesis of 1, 2, 4, 5-tetrasubstituted 1*H*-imidazole derivatives: State of the art. *Adv. Synth. Catal.* **361**, 2737–2803 (2019).
4. Wan, K. T. & Davis, M. E. Design and synthesis of a heterogeneous asymmetric catalyst. *Nature* **370**, 449–450 (1994).
5. Li, F. & Xia, C. Synthesis of 2-oxazolidinone catalyzed by palladium on charcoal: A novel and highly effective heterogeneous catalytic system for oxidative cyclocarbonylation of *β*-aminoalcohols and 2-aminophenol. *J. Catal.* **227**, 542–546 (2004).
6. Du, M. *et al.* An efficient and recyclable $AgNO_3$/ionic liquid system catalyzed atmospheric $CO_2$ utilization: Simultaneous synthesis of 2-oxazolidinones and *α*-hydroxyl ketones. *J. Catal.* **393**, 70–82 (2021).
7. Maspoch, D., Ruiz-Molina, D. & Veciana, J. Magnetic nanoporous coordination polymers. *J. Mater. Chem. A* **14**, 2713–2723 (2004).
8. Torad, N. L. *et al.* Direct synthesis of MOF-derived nanoporous carbon with magnetic Co nanoparticles toward efficient water treatment. *Small* **10**, 2096–2107 (2014).
9. Zhu, Y., Zhao, W., Chen, H. & Shi, J. A simple one-pot self-assembly route to nanoporous and monodispersed $Fe_3O_4$ particles with oriented attachment structure and magnetic property. *J. Phys. Chem. C* **111**, 5281–5285 (2007).
10. Peller, M., Böll, K., Zimpel, A. & Wuttke, S. Metal-organic framework nanoparticles for magnetic resonance imaging. *Inorg. Chem. Front.* **5**, 1760–1779 (2018).
11. Taylor, K. M., Rieter, W. J. & Lin, W. Manganese-based nanoscale metal-organic frameworks for magnetic resonance imaging. *J. Am. Chem. Soc.* **130**, 14358–14359 (2008).
12. Zhu, L., Liu, X. Q., Jiang, H. L. & Sun, L. B. Metal-organic frameworks for heterogeneous basic catalysis. *Chem. Rev.* **117**, 8129–8176 (2017).
13. Martín, N., Dusselier, M., De Vos, D. E. & Cirujano, F. G. Metal-organic framework derived metal oxide clusters in porous aluminosilicates: A catalyst design for the synthesis of bioactive aza-heterocycles. *ACS Catal.* **9**, 44–48 (2018).
14. Dang, H. V. *et al.* Copper-catalyzed one-pot domino reactions via C–H bond activation: Synthesis of 3-aroylquinolines from 2-aminobenzylalcohols and propiophenones under metal–organic framework catalysis. *RSC Adv.* **8**, 31455–31464 (2018).
15. Mirhosseini-Eshkevari, B., Esnaashari, M. & Ghasemzadeh, M. A. Novel bronsted acidic ionic liquids confined in UiO-66 nanocages for the synthesis of dihydropyrido [2, 3-*d*] pyrimidine derivatives under solvent-free conditions. *ACS Omega* **4**, 10548–10557 (2019).
16. Rechac, V. L., Cirujano, F. G., Corma, A. & Llabres I Xamena, F. X. Diastereoselective synthesis of pyranoquinolines on zirconium-containing UiO-66 metal-organic frameworks. *Eur. J. Inorg. Chem.* **2016**, 4512–4516 (2016).
17. Sepehrmansourie, H. Metal-organic frameworks (MOFs): As multi-purpose catalysts. *Iran. J. Catal.* **11**, 207–215 (2021).
18. Kalhor, S. *et al.* Anodic electrosynthesis of MIL-53(Al)-N $(CH_2PO_3H_2)_2$ as a mesoporous catalyst for synthesis of novel (*N*-methylpyrrol)-pyrazolo [3,4-*b*] pyridines via a cooperative vinylogous anomeric based oxidation. *Sci. Rep.* **11**, 19370 (2021).
19. Farhadi, S., Ghasemzadeh, M. A. & Aghaei, S. S. $NiCo_2O_4$@Ni(BDC) nano-porous metal-organic framework as a novel catalyst for the synthesis of spiro[indene[1,2-*d*]pyrimidine-ones and investigation of their antimicrobial activities. *ChemistrySelect* **4**, 729–736 (2019).
20. Truong, T., Nguyen, C. V., Truong, N. T. & Phan, N. T. Ligand-free *N*-arylation of heterocycles using metal-organic framework $[Cu(INA)_2]$ as an efficient heterogeneous catalyst. *RSC Adv.* **5**, 107547–107556 (2015).
21. Liu, J. *et al.* Applications of metal-organic frameworks in heterogeneous supramolecular catalysis. *Chem. Soc. Rev.* **43**, 6011–6061 (2014).
22. Rather, R. A. & Siddiqui, Z. N. Silver phosphate supported on metal-organic framework ($Ag_3PO_4$@MOF-5) as a novel heterogeneous catalyst for green synthesis of indenoquinolinediones. *Appl. Organomet. Chem.* **33**, e5176 (2019).
23. Tourani, H., Naimi-Jamal, M. R., Panahi, L. & Dekamin, M. G. Nanoporous metal-organic framework $Cu_2(BDC)_2(DABCO)$ as an efficient heterogeneous catalyst for one-pot facile synthesis of 1, 2, 3-triazole derivatives in ethanol: Evaluating antimicrobial activity of the novel derivatives. *Sci. Iran.* **26**, 1485–1496 (2019).
24. Ghasemzadeh, M. A., Mirhosseini-Eshkevari, B., Tavakoli, M. & Zamani, F. Metal-organic frameworks: Advanced tools for multicomponent reactions. *Green Chem.* **22**, 7265–7300 (2020).
25. Huang, S., Kou, X., Shen, J., Chen, G. & Ouyang, G. "Armor-Plating" enzymes with metal-organic frameworks (MOFs). *Angew. Chem. Int. Ed.* **59**, 8786–8798 (2020).
26. Li, J. R., Kuppler, R. J. & Zhou, H. C. Selective gas adsorption and separation in metal-organic frameworks. *Chem. Soc. Rev.* **38**, 1477–1504 (2009).
27. Alhamami, M., Doan, H. & Cheng, C. H. A review on breathing behaviors of metal-organic-frameworks (MOFs) for gas adsorption. *Materials* **7**, 3198–3250 (2014).
28. Bedia, J. *et al.* A review on the synthesis and characterization of metal organic frameworks for photocatalytic water purification. *Catalysts* **9**, 52 (2019).
29. Zheng, H. *et al.* One-pot synthesis of metal-organic frameworks with encapsulated target molecules and their applications for controlled drug delivery. *J. Am. Chem. Soc.* **138**, 962–968 (2016).
30. Argyle, M. D. & Bartholomew, C. H. Heterogeneous catalyst deactivation and regeneration: A review. *Catalysts* **5**, 145–269 (2015).
31. Maleki, A., Hajizadeh, Z. & Salehi, P. Mesoporous halloysite nanotubes modified by $CuFe_2O_4$ spinel ferrite nanoparticles and study of its application as a novel and efficient heterogeneous catalyst in the synthesis of pyrazolopyridine derivatives. *Sci. Rep.* **9**, 1–8 (2019).
32. Bhanja, P., Modak, A. & Bhaumik, A. Supported porous nanomaterials as efficient heterogeneous catalysts for $CO_2$ fixation reactions. *Chem. Eur. J.* **24**, 7278–7297 (2018).
33. Gunasekar, G. H., Shin, J., Jung, K. D., Park, K. & Yoon, S. Design strategy toward recyclable and highly efficient heterogeneous catalysts for the hydrogenation of $CO_2$ to formate. *ACS Catal.* **8**, 4346–4353 (2018).
34. Pascanu, V., González Miera, G., Inge, A. K. & Martín-Matute, B. Metal-organic frameworks as catalysts for organic synthesis: A critical perspective. *J. Am. Chem. Soc.* **141**, 7223–7234 (2019).
35. Dhakshinamoorthy, A., Alvaro, M. & Garcia, H. Metal-organic frameworks (MOFs) as heterogeneous catalysts for the chemoselective reduction of carbon-carbon multiple bonds with hydrazine. *Adv. Synth. Catal.* **351**, 2271–2276 (2009).
36. Qi, C., Ramella, D., Wensley, A. M. & Luan, Y. A Metal-organic framework brønsted acid catalyst: Synthesis, characterization and application to the generation of quinone methides for [4+2] cycloadditions. *Adv. Synth. Catal.* **358**, 2604–2611 (2016).

37. Kang, Y. S. *et al.* Metal-organic frameworks with catalytic centers: From synthesis to catalytic application. *Coord. Chem. Rev.* **378**, 262–280 (2019).
38. Timofeeva, M. N. *et al.* Metal-organic frameworks as efficient catalytic systems for the synthesis of 1, 5-benzodiazepines from 1, 2-phenylenediamine and ketones. *J. Catal.* **354**, 128–137 (2017).
39. Kumar, G. *et al.* Covalently hooked EOSIN-Y in a Zr(IV) framework as visible-light mediated, heterogeneous photocatalyst for efficient CH functionalization of tertiary amines. *J. Catal.* **371**, 298–304 (2019).
40. Wu, Y. *et al.* Metal-organic framework coated $Fe_3O_4$ magnetic nanoparticles with peroxidase-like activity for colorimetric sensing of cholesterol. *Sens. Actuators B* **249**, 195–202 (2017).
41. Yin, L. L., Kong, X. Y., Zhang, Y. & Ji, Y. Q. Facile synthesis of the magnetic metal organic framework $Fe_3O_4$@UiO-66-$NH_2$ for separation of strontium. *Biomed. Environ. Sci.* **31**, 483–488 (2018).
42. Sepehrmansourie, H., Zarei, M., Zolfigol, M. A., Babaee, S. & Rostamnia, S. Application of novel nanomagnetic metal-organic frameworks as a catalyst for the synthesis of new pyridines and 1, 4-dihydropyridines via a cooperative vinylogous anomeric based oxidation. *Sci. Rep.* **11**, 5279 (2021).
43. Gao, G., Di, J. Q., Zhang, H. Y., Mo, L. P. & Zhang, Z. H. A magnetic metal-organic framework material as a highly efficient and recyclable catalyst for synthesis of cyclohexenone derivatives. *J. Catal.* **387**, 39–46 (2020).
44. Zhang, M., Liu, Y. H., Shang, Z. R., Hu, H. C. & Zhang, Z. H. Supported molybdenum on graphene oxide/$Fe_3O_4$: An efficient, magnetically separable catalyst for one-pot construction of spiro-oxindole dihydropyridines in deep eutectic solvent under microwave irradiation. *Catal. Commun.* **88**, 39–44 (2017).
45. Chen, M. N., Mo, L. P., Cui, Z. S. & Zhang, Z. H. Magnetic nanocatalysts: synthesis and application in multicomponent reactions. *Curr. Opin. Green Sustain. Chem.* **15**, 27–37 (2019).
46. Shiri, M., Zolfigol, M. A., Kruger, H. G. & Tanbakouchian, Z. Bis-and trisindolylmethanes (BIMs and TIMs). *Chem. Rev.* **110**, 2250–2293 (2010).
47. Shiri, M. Indoles in multicomponent processes (MCPs). *Chem. Rev.* **112**, 3508–3549 (2012).
48. Arshad, M., Shoeb Khan, M., Asghar Nami, S. A. & Ahmad, D. Synthesis, characterization, computational, antimicrobial screening, and MTT assay of thiazolidinone derivatives containing the indole and pyridine moieties. *Russ. J. Gen. Chem.* **88**, 2154–2162 (2018).
49. Desai, N. C. *et al.* Synthesis, biological evaluation and molecular docking study of some novel indole and pyridine based 1, 3, 4-oxadiazole derivatives as potential antitubercular agents. *Bioorg. Med. Chem. Lett.* **26**, 1776–1783 (2016).
50. Grivsky, E. M., Lee, S., Sigel, C. W., Duch, D. S. & Nichol, C. A. Synthesis and antitumor activity of 2, 4-diamino-6-(2, 5-dimethoxybenzyl)-5-methylpyrido [2,3-*d*] pyrimidine. *J. Med. Chem.* **23**, 327–329 (1980).
51. Deb, M. L. & Bhuyan, P. J. Synthesis of novel classes of pyrido[2,3-*d*]-pyrimidines, pyrano[2,3-*d*]pyrimidines, and pteridines. *Synth. Commun.* **36**, 3085–3090 (2006).
52. Allais, C., Grassot, J. M., Rodriguez, J. & Constantieux, T. Metal-free multicomponent syntheses of pyridines. *Chem. Rev.* **114**, 10829–10868 (2014).
53. El-Borai, M. A., Rizk, H. F., Abd-Aal, M. F. & El-Deeb, I. Y. Synthesis of pyrazolo [3,4-*b*] pyridines under microwave irradiation in multi-component reactions and their antitumor and antimicrobial activities. *Eur. J. Med. Chem.* **48**, 92–96 (2012).
54. Nikpassand, M., Fekri, L. Z. & Rahro, P. N. Catalyst-free grinding method: A new avenue for synthesis of 6-amino-3-methyl-4-aryl-1*H*-pyrazolo [3,4-*b*] pyridine-5-carbonitrile and DFT studies on the mechanistic pathway of this category of compounds. *Res. Chem. Intermed.* **45**, 1707–1719 (2019).
55. Abdul-Malik, M. A., Zaki, R. M., KamalEl-Dean, A. M. & Radwan, S. M. A concise review on the synthesis and reactions of pyrazolopyrazine heterocycles. *J. Heterocycl. Chem.* **55**, 1828–1853 (2018).
56. Juaristi, E. & Cuevas, G. Recent studies of the anomeric effect. *Tetrahedron* **48**, 5019–5087 (1992).
57. Alabugin, I. V. *et al.* Stereoelectronic power of oxygen in control of chemical reactivity: The anomeric effect is not alone. *Chem. Soc. Rev.* **50**, 10253–10345 (2021).
58. Erhardt, J. M. & Wuest, J. D. Transfer of hydrogen from orthoamides. Reduction of protons to molecular hydrogen. *J. Am. Chem. Soc.* **102**, 6363–6364 (1980).
59. Atkins, T. J. Tricyclic trisaminomethanes. *J. Am. Chem. Soc.* **102**, 6364–6365 (1980).
60. Erhardt, J. M., Grover, E. R. & Wuest, J. D. Transfer of hydrogen from orthoamides. Synthesis, structure, and reactions of hexahydro-6bH-2a, 4a, 6a-triazacyclopenta [cd] pentalene and perhydro-3a, 6a, 9a-triazaphenalene. *J. Am. Chem. Soc.* **102**, 6365–6369 (1980).
61. Brunet, P. & Wuest, J. D. Formal transfers of hydride from carbon-hydrogen bonds. Attempted generation of H2 by intramolecular protonolyses of the activated carbon-hydrogen bonds of dihydrobenzimidazoles. *Can. J. Chem.* **74**, 689–496 (1996).
62. Zolfigol, M. A., Afsharnadery, F., Baghery, S., Salehzadeh, S. & Maleki, F. Catalytic applications of {[HMIM]C($NO_2$)$_3$}: As a nano ionic liquid for the synthesis of pyrazole derivatives under green conditions and a mechanistic investigation with a new approach. *RSC Adv.* **5**, 75555–75568 (2015).
63. Zolfigol, M. A. *et al.* Silica vanadic acid [$SiO_2$-VO($OH$)$_2$] as an efficient heterogeneous catalyst for the synthesis of 1, 2-dihydro-1-aryl-3 *H*-naphth [1,2-*e*][1,3] oxazin-3-one and 2, 4, 6-triarylpyridine derivatives via anomeric based oxidation. *RSC Adv.* **5**, 100546–100559 (2015).
64. Yarie, M. Catalytic anomeric based oxidation. *Iran. J. Catal.* **7**, 85–88 (2017).
65. Yarie, M. Catalytic vinylogous anomeric based oxidation. *Iran. J. Catal.* **10**, 79–83 (2020).
66. Férey, G. *et al.* A chromium terephthalate-based solid with unusually large pore volumes and surface area. *Science* **309**, 2040–2042 (2005).
67. Rostamnia, S., Alamgholiloo, H. & Jafari, M. Ethylene diamine post-synthesis modification on open metal site Cr-MOF to access efficient bifunctional catalyst for the Hantzsch condensation reaction. *Appl. Organomet. Chem.* **32**, e4370 (2018).
68. Babaee, S., Zarei, M., Sepehrmansourie, H., Zolfigol, M. A. & Rostamnia, S. Synthesis of metal-organic frameworks MIL-101(Cr)-$NH_2$ containing phosphorous acid functional groups: Application for the synthesis of *N*-amino-2-pyridone and pyrano [2,3-*c*] pyrazole derivatives via a cooperative vinylogous anomeric-based oxidation. *ACS Omega* **5**, 6240–6249 (2020).
69. Slaett, J., Romero, I. & Bergman, J. Cyanoacetylation of indoles, pyrroles and aromatic amines with the combination cyanoacetic acid and acetic anhydride. *Synthesis* **16**, 2760–2765 (2004).
70. Ahmad, I., Mishra, N. K. & Ghosh, T. 5-(1*H*-Indol-3-yl)-pyrazolyl derivatives as colorimetric sensor for anions. *J. Incl. Phenom. Macrocycl. Chem.* **76**, 183–191 (2013).
71. Karimi, F., Yarie, M. & Zolfigol, M. A. Synthesis and characterization of $Fe_3O_4$@$SiO_2$@$(CH_2)_3NH(CH_2)_2O_2P(OH)_2$ and its catalytic application in the synthesis of benzo-[*h*] quinoline-4-carboxylic acids via a cooperative anomeric based oxidation mechanism. *Mol. Catal.* **489**, 110924 (2020).
72. Afsar, J. *et al.* Synthesis and application of melamine-based nano catalyst with phosphonic acid tags in the synthesis of (3′-indolyl) pyrazolo [3,4-*b*] pyridines via vinylogous anomeric based oxidation. *Mol. Catal.* **482**, 110666 (2020).
73. Jalili, F., Zarei, M., Zolfigol, M. A., Rostamnia, S. & Moosavi-Zare, A. R. SBA-15/PrN ($CH_2PO_3H_2$)$_2$ as a novel and efficient mesoporous solid acid catalyst with phosphorous acid tags and its application on the synthesis of new pyrimido [4,5-*b*] quinolones and pyrido [2,3-*d*] pyrimidines via anomeric based oxidation. *Microporous Mesoporous Mater.* **294**, 109865 (2020).

74. Ghasemi, P., Yarie, M., Zolfigol, M. A. & Taherpour, A. A. Ionically tagged magnetic nanoparticles with urea linkers: Application for preparation of 2-aryl-quinoline-4-carboxylic acids via an anomeric-based oxidation mechanism. *ACS Omega* **5**, 3207–3217 (2020).
75. Karimi, F., Yarie, M. & Zolfigol, M. A. A convenient method for synthesis of terpyridines via a cooperative vinylogous anomeric based oxidation. *RSC Adv.* **10**, 25828–25835 (2020).
76. Dashteh, M. *et al.* Synthesis of cobalt tetra-2,3-pyridiniumporphyrazinato with sulfonic acid tags as an efficient catalyst and its application for the synthesis of bicyclic ortho-aminocarbonitriles, cyclohexa-1, 3-dienamines and 2-amino-3-cyanopyridines. *RSC Adv.* **10**, 27824–27834 (2020).
77. Karimi, F., Yarie, M. & Zolfigol, M. A. $Fe_3O_4$@$SiO_2$@$(CH_2)_3$-urea-thiourea: a novel hydrogen-bonding and reusable catalyst for the construction of bipyridine-5-carbonitriles via a cooperative vinylogous anomeric based oxidation. *Mol. Catal.* **489**, 111201 (2020).
78. Torabi, M. *et al.* Synthesis of new pyridines with sulfonamide moiety via a cooperative vinylogous anomeric-based oxidation mechanism in the presence of a novel quinoline-based dendrimer-like ionic liquid. *RSC Adv.* **11**, 3143–3152 (2021).
79. Zolfigol, M. A. *et al.* A highly stable and active magnetically separable Pd nanocatalyst in aqueous phase heterogeneously catalyzed couplings. *Green Chem.* **15**, 2132–2140 (2013).
80. Babaee, S., Zolfigol, M. A., Zarei, M. & Zamanian, J. 1, 10-Phenanthroline-based molten salt as a bifunctional sulfonic acid catalyst: Application to the synthesis of *N*-heterocycle compounds via anomeric based oxidation. *ChemistrySelect* **3**, 8947–8954 (2018).
81. Kalhor, S. *et al.* Novel uric acid-based nano organocatalyst with phosphorous acid tags: Application for synthesis of new biologically-interest pyridines with indole moieties via a cooperative vinylogous anomeric based oxidation. *Mol. Catal.* **507**, 111549 (2021).
82. Sepehrmansourie, H., Zarei, M., Taghavi, R. & Zolfigol, M. A. Mesoporous ionically tagged cross-linked poly(vinyl imidazole)s as novel and reusable catalysts for the preparation of *N*-heterocycle spiropyrans. *ACS Omega* **4**, 17379–17392 (2019).
83. Moosavi-Zare, A. R., Zolfigol, M. A., Zarei, M., Khakyzadeh, V. & Hasaninejad, A. Design, characterization and application of new ionic liquid 1-sulfopyridinium chloride as an efficient catalyst for tandem knoevenagel-michael reaction of 3-methyl-1-phenyl-1*H*-pyrazol-5(4*H*)-one with aldehydes. *Appl. Catal. A* **467**, 61–68 (2013).
84. Zolfigol, M. A. Silica sulfuric acid/$NaNO_2$ as a novel heterogeneous system for production of thionitrites and disulfides under mild conditions. *Tetrahedron* **57**, 9509–9511 (2001).
85. Sepehrmansourie, H. Silica sulfuric acid (SSA): As a multipurpose catalyst. *Iran. J. Catal.* **10**, 175–179 (2020).
86. Sepehrmansouri, H. *et al.* Multilinker phosphorous acid anchored En/MIL-100(Cr) as a novel nanoporous catalyst for the synthesis of new *N*-heterocyclic pyrimido [4,5-*b*] quinolines. *Mol. Catal.* **481**, 110303 (2020).
87. Zarei, M., Sepehrmansourie, H., Zolfigol, M. A., Karamian, R. & Moazzami Farida, S. H. Novel nano-size and crab-like biological-based glycoluril with sulfonic acid tags as a reusable catalyst: Its application to the synthesis of new mono-and bis-spiropyrans and their in vitro biological studies. *New. J. Chem.* **42**, 14308–14317 (2018).


## Acknowledgements

We thank the Bu-Ali Sina University and Iran National Science Foundation (INSF) (Grant Number: 4004528) for financial support.

## Author contributions

H.S. and S.B.; methodology, validation, investigation. M.Z. investigation and writing the original draft. M.A.Z.; supervision, resources, project administration, funding acquisition, conceptualization, writing-review. S.R. and S.A. writing-review and editing.

## Competing interests

The authors declare no competing interests.

## Additional information

**Supplementary Information** The online version contains supplementary material available at https://doi.org/10.1038/s41598-022-17879-5.

**Correspondence** and requests for materials should be addressed to M.Z. or M.A.Z.

**Reprints and permissions information** is available at www.nature.com/reprints.

**Publisher's note** Springer Nature remains neutral with regard to jurisdictional claims in published maps and institutional affiliations.

**Open Access** This article is licensed under a Creative Commons Attribution 4.0 International License, which permits use, sharing, adaptation, distribution and reproduction in any medium or format, as long as you give appropriate credit to the original author(s) and the source, provide a link to the Creative Commons licence, and indicate if changes were made. The images or other third party material in this article are included in the article's Creative Commons licence, unless indicated otherwise in a credit line to the material. If material is not included in the article's Creative Commons licence and your intended use is not permitted by statutory regulation or exceeds the permitted use, you will need to obtain permission directly from the copyright holder. To view a copy of this licence, visit http://creativecommons.org/licenses/by/4.0/.

© The Author(s) 2022